Monte Carlo Simulation of Long Chain Polymer Melts: Crossover from Rouse to Reptation Dynamics

T. Kreer,*,† J. Baschnagel,‡ M. Müller,† and K. Binder†

Institut für Physik, Johannes-Gutenberg Universität, D-55099 Mainz, Germany; and Institut Charles Sadron, 6 rue Boussingault, F-67083, Strasbourg Cedex, France

Received August 28, 2000; Revised Manuscript Received November 28, 2000

ABSTRACT: We present data from Monte Carlo simulations for monodisperse linear polymer chains in dense melts with degrees of polymerization between $N = 16$ and $N = 512$. The aim of this study is to investigate the crossover from Rouse-like dynamics for short chains to reptation-like dynamics for long chains. To address this problem, we calculate a variety of different quantities: standard mean-square displacements of inner monomers and of the chain's center of mass, the recently proposed cubic invariant (Ebert, U.; et al. *Phys. Rev. Lett.* **1997**, *78*, 1592), persistence of bond-vector orientation with time, and the autocorrelation functions of the bond vector, the end-to-end vector, and the Rouse modes. This analysis reveals that the crossover from nonentangled to entangled dynamics is very protracted. Even the biggest chain length $N = 512$, which is about 14 times larger than the entanglement length, shows no clear evidence for reptation. In the opposite limit of short chains, no pure Rouse behavior is found either. Local stiffness effects have to be taken into account.

I. Introduction

A detailed description of the slow dynamics of entangled polymer chains would be of great interest for better understanding the physical properties of dense polymer melts or solutions. Several attempts to solve this problem have been made. In a seminal paper, de Gennes introduced the concept of reptation.[1] The fundamental idea is that the motion of a polymer is not spatially isotropic, but has to occur along the contour of a "tube" which is formed by the surrounding chains. These surrounding chains are treated as a fixed network of impenetrable obstacles. The simultaneous motion of the polymers and possible correlations resulting from that are disregarded. The elaboration of this idea has led to a rich scenario of testable predictions.[2−4] Critical analyses of these predictions by experiments[5−9] and computer simulations[10−12] suggest that reptation is an important relaxation mechanism. However, it cannot provide a quantitative explanation of all dynamic features observed. These deviations could result from additional relaxation processes which blur the clear signature of reptation for typical experimental chain lengths N and become negligible only in the asymptotic limit of extremely large N (see ref 13, however, for a different asymptotic behavior).

The additional relaxation mechanisms could involve fluctuations of the tube's contour,[14−16] reorganization of the tube[17] by release and creation of topological constraints,[5,14,18] elastic distortions of the entanglement network,[19] or long-lived density fluctuations.[20] All these extensions assume the existence of a tube. None of them explains its microscopic origin. An attempt to develop a microscopic theory was made by the development of a mode-coupling theory for polymers.[21−26] This approach leads to similar predictions as reptation theory without invoking a tube hypothesis.

* To whom correspondence should be addressed. E-mail: tkreer@plato.physik.uni-mainz.de.
† Johannes-Gutenberg Universität.
‡ Institut Charles Sadron.

However, some doubt was cast on this concept by simulations of a model by Shaffer,[27] which respects excluded volume interactions between the monomers of the chains but allows Monte Carlo moves that lead to intersections between bonds connecting the monomers. For long chains in this model a simple Rouse-like behavior is found. Only when the conditions that bonds must not intersect is used as an additional constraint in the dynamics, a reptation-like behavior results from the simulation. These results, where static correlations are precisely identical for both models, but one dynamic version exhibits Rouse behavior and the other reptation-like behavior, seem to imply that the topological constraint of the noncrossability of chains is not an automatic consequence of the excluded volume interaction. In this context, we note that many other attempts have been made to account for the slow dynamics of entangled polymer chains by concepts differing from reptation, e.g., collective motion of many entangled chains,[28] but we are not attempting to critically evaluate all these theories here.

In view of these diverse attempts to improve on reptation theory, it is also beneficial to consider a model which exhibits pure reptation behavior in the asymptotic limit of large chains and long times, and for which finite-N and finite-time corrections can be calculated. Evans and Edwards proposed such a model in which a single chain moves through a regular array of impenetrable obstacles.[29] The obstacles do not influence the equilibrium configuration of the chain, but only the accessible relaxation moves of its monomers. This model has recently been reanalyzed analytically.[30,31] Detailed comparisons with computer simulations[30,32,33] reveal an extremely slow crossover to the asymptotic power laws characteristic of reptation. Even in the ideal situation, where the tube diameter is equal to the bond length, the power laws only become clearly pronounced for $N > 100$. If the lattice of obstacles is diluted, the tube diameter increases and the crossover to reptation is shifted to larger chain lengths.[33]

10.1021/ma001500f CCC: $20.00
Published on Web 01/20/2001

Table 1. Chain Length Dependence of the Size of a Chain and of Its Relaxation Times[a]

N	R_e^2	R_g^2	$\langle\lambda_1\rangle$:$\langle\lambda_2\rangle$:$\langle\lambda_3\rangle$	τ_b	τ_{ee}	τ_1
16	136	23	12.42:2.78:1	391	15 180	14 519
32	293	49	12.30:2.74:1	454	78 509	76 879
64	607	102	12.17:2.71:1	430	367 863	384 993
128	1314	217	11.88:2.67:1	445	2 387 464	2 558 552
512	5348	885	11.87:2.65:1	461	214 679 565	233 045 839

[a] R_e^2 = mean-square end-to-end vector, R_g^2 = mean-square radius of gyration, $\langle\lambda_\alpha\rangle$ = mean eigenvalue of the gyration tensor in spatial direction α (=1, 2, 3) (see eq 1), τ_b = relaxation time of the bond vector defined by $\phi_b(\tau_b) = 1/e$, τ_{ee} relaxation time of the end-to-end vector defined by eq 21, and τ_1 = relaxation time of the first Rouse mode defined by $\phi_1(\tau_1) = 1/e$. Our ratios for the eigenvalues $\langle\lambda_\alpha\rangle$ are close to those for Gaussian chains: $\langle\lambda_1\rangle$:$\langle\lambda_2\rangle$:$\langle\lambda_3\rangle$ = 12.07:2.72:1[47] (see also ref 46).

The latter study resembles more closely the situation encountered in computer simulations of melts where the tube diameter is in general larger than the bond length. Taking into account that simulations typically work with $N < 1000$, the analysis of the Evans−Edwards model suggests that the results of polymer melt simulations are characteristic of the crossover from nonentangled, Rouse-like dynamics for short chains to (slightly) entangled, reptation-like dynamics for long chains. With the present study, we want to further investigate this crossover by a Monte Carlo simulation of the bond-fluctuation model. To analyze the simulation data we will use Rouse and reptation theories.

Our paper is organized as follows: Section II introduces the model and describes some of its static properties. Section III represents the main part of the paper. It deals with dynamics of the model. Here, we compare various mean-square displacements and orientational correlation functions, extract the chain length dependence of relaxation times and of the diffusion coefficient, and estimate the parameters of reptation theory, such as the tube diameter or the entanglement length. The final section, section IV, summarizes our conclusions.

II. Model and Static Properties

The aim of the present work is to extend and to complement previous studies of the crossover from Rouse to reptation dynamics using the bond-fluctuation model.[34−36] The bond-fluctuation model is a coarse-grained lattice model,[12,37,38] in which a polymer is represented by a chain consisting of N monomers. Each monomer occupies a unit cell of a simple cubic lattice (unit cell = eight lattice sites). This increased monomer size allows the bond vectors $\boldsymbol{l}$ to vary in both length and direction to a much larger extent than in simpler lattice models where a monomer is associated with a single site.[37] In total, there are 108 bond vectors[39] giving rise to 87 bond angles and 5 different bond lengths (2, $\sqrt{5}$, $\sqrt{6}$, 3, $\sqrt{10}$). The average bond length and bond angle depend on the volume fraction, $\phi = 8NP/L^3$, of occupied lattice sites (P = total number of polymers in the simulation box; L = linear dimension of the box). In the present study, we choose $\phi = 0.5$. This choice guarantees that the model realizes typical properties of dense melts.[34] For $\phi = 0.5$ the mean bond length and mean cosine of the bond angle are given by $l = \langle\boldsymbol{l}^2\rangle^{1/2} = 2.64$ and $\alpha = \langle\cos\theta\rangle = -0.1055$, respectively.[40]

To analyze the change in dynamic behavior with increasing N simulations were performed for different chain lengths ranging from $N = 16$ to $N = 512$ (see Table 1). This extends previous studies[34] by a factor of 2 only, but it amounts to an increase in relaxation time by almost an order of magnitude (cf. Table 1). Furthermore, the system size could also be chosen much larger. For most chain lengths the linear dimension of the simulation box is more than a factor of 2 greater than the average end-to-end distance R_e, i.e., $L > 2R_e$ (with the exception of $N = 512$ where $L = 128 \simeq 1.75R_e$ only; see Table 1). Since finite-size effects may be expected if $L \leq 2R_e$, Figure 1 compares the mean-square end-to-end distance R_e^2 and mean-square radius of gyration R_g^2 of the present study with the values of earlier works.[34,35] Two conclusions can be drawn from this figure. First, finite-size effects did not affect previous (static) results. Within the statistical uncertainties the old data for $N = 200$ ($R_e \simeq 45$, $L = 40$[34]) agree with the present analysis. Second, the bond-fluctuation model approaches the asymptotic ideal chain limit, i.e., $R_e^2 = 6R_g^2 = C_\infty l^2(N-1)$, if $N > 100$. Here, C_∞ ($= \lim_{N\to\infty} R_e^2/[(N-1)l^2]$) is the characteristic ratio which measures the swelling of a chain due to its intrinsic stiffness compared to a pure random walk. Using $C_\infty \simeq 1.56$ (see Figure 1) and $l_p = l(C_\infty + 1)/2$[41], the persistence length, l_p, of the model is given by $l_p \simeq 3.38$.

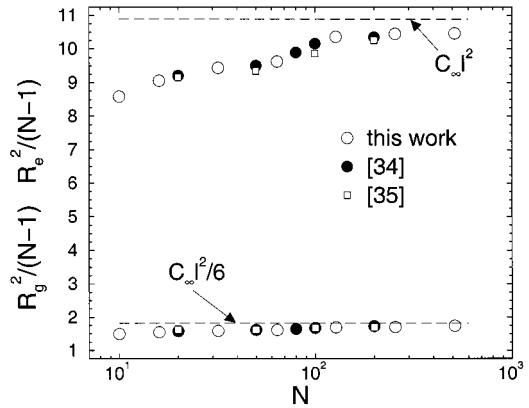

Figure 1. Mean-square end-to-end vector, R_e^2 (upper symbols), and radius of gyration, R_g^2 (lower symbols), plotted against chain length N. Asymptotically, both quantities are expected to behave as $R_e^2 = C_\infty l^2(N-1)$ and $R_g^2 = C_\infty l^2(N-1)/6$ for dense melts. Here, $l = \langle\boldsymbol{l}^2\rangle^{1/2}$ (=2.64) is the mean bond length and C_∞ the characteristic ratio at infinite chain length. The value of $C_\infty \simeq 1.56$ was obtained by an extrapolation of $R_e^2/(N-1)l^2$ to $N \to \infty$ using $N > 100$. Both R_e^2 and R_g^2 enter the asymptotic regime if $N > 100$ (for R_g^2 this is hard to see on the scale of this figure; see Figure 2). Furthermore, the figure shows that the present data are consistent with previously obtained results (on smaller systems).[34,35]

The shape of a polymer is not spherical.[42−47] A good indicator of its geometrical form is the gyration tensor $\mathbf{Q}$ whose elements are given by[42−44]

$$Q_{\alpha\beta} = \frac{1}{N}\sum_{n=1}^{N}(R_{\alpha,n} - R_{\mathrm{cm},\alpha})(R_{\beta,n} - R_{\mathrm{cm},\beta}) \qquad (\alpha,\beta = 1,...,3) \quad (1)$$

Here, $R_{\alpha,n}$ and $R_{\mathrm{cm},\alpha}$ denote the αth-component of the position vectors to monomer n and to the chain's center of mass, i.e., $\boldsymbol{R}_n = (R_{1,n}, R_{2,n}, R_{3,n})$ and $\boldsymbol{R}_{\mathrm{cm}} = (R_{\mathrm{cm},1}, R_{\mathrm{cm},2}, R_{\mathrm{cm},3})$. The trace of this tensor provides another way to calculate the radius of gyration[42]

$$\langle \mathrm{Tr}\ \mathbf{Q}\rangle = \langle\lambda_1\rangle + \langle\lambda_2\rangle + \langle\lambda_3\rangle = R_g^2 \qquad (2)$$

where λ_α are the eigenvalues of $\mathbf{Q}$. If the shape of a polymer was spherical, one would have $\langle\lambda_1\rangle = \langle\lambda_2\rangle = \langle\lambda_3\rangle$.

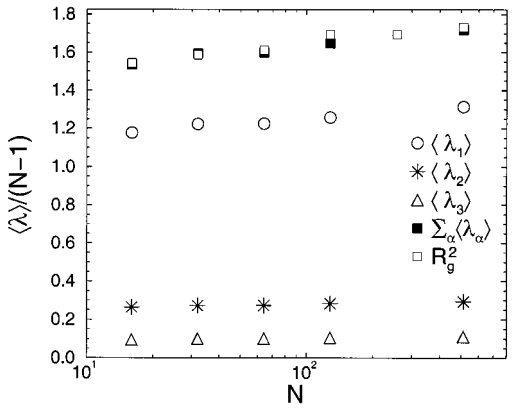

Figure 2. Eigenvalues, $\langle\lambda_\alpha\rangle/(N-1)$ ($\alpha = 1, 2, 3$), of the gyration tensor **Q** (eq 1) plotted vs chain length N. If the shape of a polymer were spherical, one would have $\langle\lambda_1\rangle = \langle\lambda_2\rangle = \langle\lambda_3\rangle$. The result $\langle\lambda_1\rangle \gg \langle\lambda_2\rangle > \langle\lambda_3\rangle$ shows that it instead resembles a flattened ellipsoid ("prolate" chains). The ratio of the eigenvalues ($\langle\lambda_1\rangle:\langle\lambda_2\rangle:\langle\lambda_3\rangle = 11.87:2.65:1$ for $N = 512$) is fairly close to that expected for random walks (12.07:2.72:1[46]). As anticipated from eq 2, the eigenvalues sum up to the radius of gyration calculated independently by $R_g^2 = \sum_{n=1}^{N} (\boldsymbol{R}_n - \boldsymbol{R}_{cm})^2/N$, where $\boldsymbol{R}_n$ and $\boldsymbol{R}_{cm}$ are the position vectors of the nth monomer and of the center of mass, respectively.

Contrary to that, Figure 2 shows that the biggest eigenvalue, $\langle\lambda_1\rangle$, is much larger than the other two eigenvalues. This implies that the shape of a chain is distorted with respect to a sphere: It is stretched in direction of the long principal axis and shrunk in directions of the axes corresponding to $\langle\lambda_2\rangle$ and $\langle\lambda_3\rangle$. Therefore, a chain rather resembles a "flattened American football". [Recent studies[46,47] of the shape of Gaussian chains indicate that the visualization of a random-walk polymer as a flattened American football is not completely correct. The density distribution of monomers in the coordinate system of the principal axes exhibits a slight minimum at the origin (i.e., at the center of mass) for the largest axis, whereas it has a maximum for the other two axes. Therefore, the shape is rather dumbbell-like.] This characteristic property can be exploited to construct an efficient coarse-grained model for dense polymer melts.[48,49]

In the course of the simulation, a monomer and a lattice direction (out of six) are selected at random, and a jump by one lattice constant is attempted in that direction. The jump is accepted if the resulting bond vectors belong to the allowed set of bonds and if the targeted lattice sites are empty. Otherwise, the move is rejected. This random displacement simulates the impact of a stochastic force which is exerted on a monomer by its local environment.

In the single chain limit, this local jump model is expected to give rise to Rouse dynamics if hydrodynamic interactions are absent.[4] Since hydrodynamic forces are mediated by solvent molecules, an isolated chain of the bond-fluctuation model provides an example for this conjecture.[12,36] However, if the volume fraction ϕ increases, deviations from Rouse dynamics are observed due to the mutual interaction of the chains and due to the onset of entanglements.[12] Nevertheless, the Rouse model is generally believed to provide a reliable description of short (nonentangled) chains in a melt. Therefore, we determined its basic variables, the Rouse modes[50]

$$\boldsymbol{X}_p(t) = \frac{1}{N}\sum_{n=1}^{N} \boldsymbol{R}_n(t) \cos\frac{(n-{}^1/_2)p\pi}{N} \qquad (p = 0,1,...,N-1) \quad (3)$$

where $\boldsymbol{R}_n(t)$ is the position of the nth monomer at time t. At $t = 0$ the (static) correlation of the modes reflects the structural properties of the polymers. For ideal random walk chains it is given by[50]

$$\langle \boldsymbol{X}_p(0)\cdot\boldsymbol{X}_q(0)\rangle = \delta_{pq}\frac{b^2}{8N}\left[\frac{1}{\sin(p\pi/2N)}\right]^2 \xrightarrow{p/N \ll 1} \delta_{pq}\frac{1}{2\pi^2}\frac{Nb^2}{p^2} \quad (\text{for } p > 0) \quad (4)$$

In this equation, b denotes the effective bond length defined by $b^2 = C_\infty l^2$.[4] However, we use $b^2 = R_e^2/(N-1)$. This ratio is (slightly) chain-length dependent. It varies from about 8.7 for $N = 16$ to about 10.6 for $N = 512$, i.e., by about 18%, in our simulation.

Using this identification eq 4 suggests that a plot of $8N(N-1)\langle \boldsymbol{X}_p(0)^2\rangle/R_e^2$ vs p/N should yield a master curve. Figure 3 shows a test of this prediction. In fact, the data for all chain lengths collapse onto a common curve which is nicely described by $[\sin(p\pi/2N)]^{-2}$ if $p/N \lesssim 0.05$. However, if p/N increases, deviations between the simulation results and the Rouse prediction gradually develop. The Rouse theory overestimates the correlation, especially for $p/N \gtrsim 0.3$. These large modes probe local distances along the backbone of a chain. For instance, $p/N \gtrsim 0.3$ corresponds to subunits of a trimer and smaller than that. On these local scales, the intrinsic stiffness of a polymer should be taken into account.

The simplest way to achieve this consists of replacing the random walk by a freely rotating chain.[4,41] This is a chain model, in which the mean bond length and bond angle are fixed and each bond is allowed to rotate freely around the direction of the preceding bond. Starting from

$$\langle \boldsymbol{X}_p{}^2(0)\rangle = \frac{1}{N^2}\sum_{n,m=1}^{N}\langle \boldsymbol{R}_n(0)\cdot\boldsymbol{R}_m(0)\rangle \cos\frac{p\pi(n-{}^1/_2)}{N}\cos\frac{p\pi(m-{}^1/_2)}{N}$$

this implies that we should write (remember $\alpha = \langle\cos\theta\rangle = -0.1055$)

$$\langle \boldsymbol{R}_n\cdot\boldsymbol{R}_m\rangle = \sum_{i=1}^{n-1}\sum_{j=1}^{m-1}\langle \boldsymbol{l}_i\cdot\boldsymbol{l}_j\rangle = l^2\sum_{i=1}^{n-1}\sum_{j=1}^{m-1}(-\alpha)^{|i-j|}$$

instead of $\langle \boldsymbol{l}_i\cdot\boldsymbol{l}_j\rangle = l^2\delta_{ij}$ for a random walk. Using furthermore

$$\sum_{n,m=2}^{N}\cos\frac{p\pi(n-{}^1/_2)}{N}\cos\frac{p\pi(m-{}^1/_2)}{N}\sum_{i=1}^{n-1}\sum_{j=1}^{m-1}(-\alpha)^{|i-j|} = \sum_{n=2}^{N}\sum_{i=2}^{n}\sum_{m=i}^{N}\cos\frac{p\pi(n-{}^1/_2)}{N}\cos\frac{p\pi(m-{}^1/_2)}{N}\times \left[\frac{(-\alpha)^{m-i+1}-1}{(-\alpha)-1}+\frac{(-\alpha)^{n-i+1}-1}{(-\alpha)-1}-1\right]$$

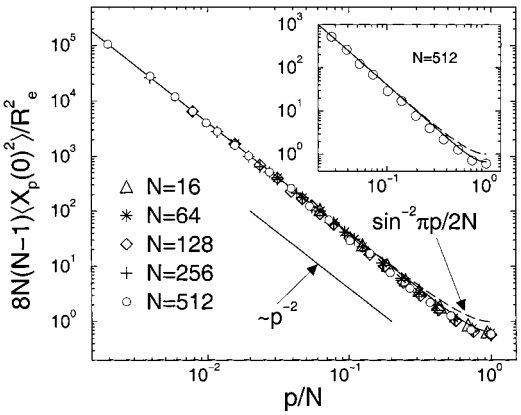

Figure 3. Rescaled static autocorrelation of the Rouse modes, $8N(N-1)\langle \boldsymbol{X}_p^2(0)\rangle/R_e^2$, vs p/N for all chain lengths studied (R_e = end-to-end distance). This rescaling is motivated by eq 4. The dashed and the solid lines show the theoretical predictions for fully flexible chains (eq 4) and for freely rotating chains (eq 5) where local stiffness due to the bond angle is taken into account. If $p/N \lesssim 0.05$ (corresponding to subchains larger than about 20 monomers), both predictions coincide and describe the simulation data well. In this case, eqs 4 and 5 are well approximated by the power law p^{-2} (indicated by a solid line in the figure). However, if $p/N > 0.3$ (corresponding to subchains smaller than about three monomers), the fully flexible (standard) Rouse model overestimates the correlation, whereas the (approximate) consideration of chain stiffness still provides a reasonable description. A magnification of the comparison between eqs 4 and 5 is shown in the inset for $N = 512$.

one obtains

$$\frac{8N(N-1)}{R_e^2}\langle \boldsymbol{X}_p^2(0)\rangle = \left[\frac{1}{\sin(p\pi/2N)}\right]^2 - \frac{4(-\alpha)}{1-2(-\alpha)\cos(p\pi/N)+(-\alpha)^2}\times \left[1+\frac{1}{N}\frac{2\alpha(1+\alpha)}{1-\alpha}\frac{1-(-1)^p(-\alpha)^N}{1+2\alpha\cos(p\pi/N)+\alpha^2}\frac{\sin(p\pi/N)}{\tan(p\pi/2N)}\right] \quad (5)$$

Equation 5 is valid if $|\alpha| < 1$. Although the second line of the equation violates the p/N scaling, its numerical value for $\alpha = -0.1055$ is always smaller than 0.03 (="worst case" for $p = 1$ and $N = 16$) and thus negligible. Therefore, we compare the first line of eq 5 to the simulation data. Figure 3 shows that the approximate consideration of stiffness by eq 5 reasonably accounts for the suppression of correlations below the Rouse prediction 4. Similar approaches are pursued in refs 51 and 52 and tested against experiments and simulations.[53,54]

Figure 4 tests another prediction of eq 4, the orthogonality of the Rouse modes, i.e., $\langle \boldsymbol{X}_p(0)\cdot\boldsymbol{X}_q(0)\rangle \sim \delta_{pq}$, for two chain lengths $N = 16$ and $N = 128$. Whereas the autocorrelation of the first mode is 1−2 orders of magnitude larger than cross-correlations with $p > 1$ for both chain lengths, this difference in magnitude is only preserved for the short chain when increasing p toward $p = N - 1$ (see Figure 4b). On the other hand, cross-correlations of the same amplitude as the self-correlation develop between $p = 127$ and the smallest modes for $N = 128$. If one interpretes a difference of 1 to 2

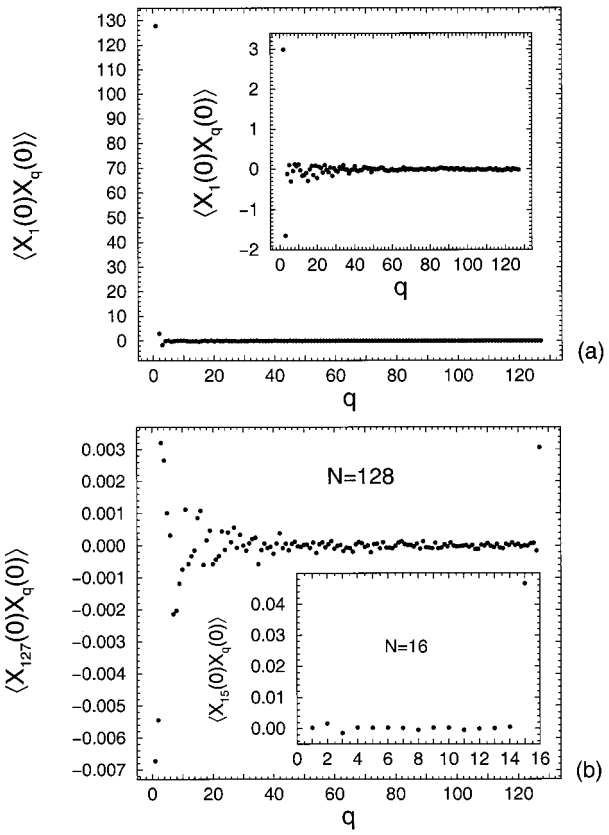

Figure 4. Test of the orthogonality of the Rouse modes at $t = 0$ (see eq 4). Panel a shows $\langle \boldsymbol{X}_1(0)\cdot\boldsymbol{X}_q(0)\rangle$ ($q = 1, ..., 127$) for $N = 128$ ($> N_e \approx 37$; N_e = entanglement length). The inset magnifies the results for $q = 2, ..., 127$. Cross-correlations between the first and the $q = 2,3$ modes are about 1−2 orders of magnitude smaller than $\langle \boldsymbol{X}_1^2(0)\rangle$, but much stronger than those for $q > 3$. If $N < N_e$, the behavior is qualitatively the same as shown in the inset. However, all correlations are more than 2 orders of magnitude smaller than the self-correlation for nonentangled chains. Panel b compares $\langle \boldsymbol{X}_p(0)\cdot\boldsymbol{X}_q(0)\rangle$ of the largest mode for $N = 128$, $\langle \boldsymbol{X}_{127}(0)\cdot\boldsymbol{X}_q(0)\rangle$, with that for $N = 16$ ($< N_e$), $\langle \boldsymbol{X}_{15}(0)\cdot\boldsymbol{X}_q(0)\rangle$. If $N > N_e$, cross-correlations with the smallest Rouse modes are as large as the self-correlation, whereas they are at least an order of magnitude smaller if $N < N_e$.

orders of magnitude between self- and cross-correlations as a numerical realization of $\langle \boldsymbol{X}_p(0)\cdot\boldsymbol{X}_q(0)\rangle \sim \delta_{pq}$, the full spectrum of Rouse modes is only δ-correlated for $N = 16$, while small and large modes interfere for large chain lengths.

III. Dynamic Properties of the Melt

This section discusses the simulation results for dynamic properties of the polymer melt. It is split into three subsections. The first deals with an analysis of various mean-square displacements. The presentation of the data is very much influenced by a recent thorough theoretical and numerical study of the Evans−Edwards model.[30−33] The second subsection presents the relaxation behavior of the correlation function of the bond-vector, of the end-to-end distance and of the Rouse modes, whereas the last subsection discusses the chain-length dependence of the corresponding relaxation times and of the diffusion coefficient.

A. Mean-Square Displacements. Important quantities used to study the crossover from Rouse to reptation dynamics are the following mean-square displacements:

$$
\begin{aligned}
g_1(t) &= \langle [\boldsymbol{R}_{N/2}(t) - \boldsymbol{R}_{N/2}(0)]^2 \rangle \\
g_2(t) &= \langle [\boldsymbol{R}_{N/2}(t) - \boldsymbol{R}_{N/2}(0) - \boldsymbol{R}_{\mathrm{cm}}(t) + \boldsymbol{R}_{\mathrm{cm}}(0)]^2 \rangle \\
g_3(t) &= \langle [\boldsymbol{R}_{\mathrm{cm}}(t) - \boldsymbol{R}_{\mathrm{cm}}(0)]^2 \rangle \\
g_4(t) &= \frac{1}{2}(\langle [\boldsymbol{R}_1(t) - \boldsymbol{R}_1(0)]^2 \rangle + \langle [\boldsymbol{R}_N(t) - \boldsymbol{R}_N(0)]^2 \rangle)
\end{aligned} \tag{6}
$$

Here, g_1 is the mean-square displacement of the inner monomer of a chain (situated at position $\boldsymbol{R}_{N/2}(t)$ at time t), g_2 is the same displacement measured relative to the motion of the chain's center of mass ($\boldsymbol{R}_{\mathrm{cm}}(t)$ is position of the center of mass at time t), $g_3(t)$ is the mean-square displacement of the center of mass, and g_4 is that of the end monomers. Within the framework of reptation theory, one expects[3,4,11,12]

$$
g_1(t) \sim \begin{cases} t^{1/2} & \text{if } t \ll \tau_{\mathrm{e}} \\ t^{1/4} & \text{if } \tau_{\mathrm{e}} \ll t \ll \tau_{\mathrm{R}} \\ (t/N)^{1/2} & \text{if } \tau_{\mathrm{R}} \ll t \ll \tau_{\mathrm{d}} \\ t/N^2 & \text{if } \tau_{\mathrm{d}} \ll t \end{cases} \tag{7}
$$

$$
g_3(t) \sim \begin{cases} t/N & \text{if } t \ll \tau_{\mathrm{e}} \\ (t/N^2)^{1/2} & \text{if } \tau_{\mathrm{e}} \ll t \ll \tau_{\mathrm{R}} \\ t/N^2 & \text{if } \tau_{\mathrm{R}} \ll t \end{cases}
$$

At early times, a chain does not feel the entanglement constraints imposed by its neighbors. Assuming the Rouse model to provide a realistic description for nonentangled chains, one expects $g_1(t) \sim t^{1/2}$ and $g_3(t) \sim t$ in this case. If t equals the entanglement time, τ_{e}, the constraints begin to dominate the polymer dynamics. For larger times, a chain moves as if it were confined in a tube created by its neighbors: It can only slide along the tube axis (the so-called "primitive path"), whereas motion perpendicular to it is suppressed. Since the tube can be thought of as an envelope around the chain's random-walk-like configuration, the chain performs Rouse dynamics along a random walk. This leads to $g_1 \sim t^{1/4}$ and $g_3 \sim t^{1/2}$. If t reaches the Rouse time, τ_{R}, the chain configuration is relaxed inside the tube. For larger times, the center of mass diffuses freely and the inner monomer begins to diffuse out of the tube. The monomer leaves the tube completely if t equals the disentanglement time, τ_{d}.

The power laws of eq 7 represent the asymptotic behavior. They can be observed clearly only for very large N, where the time scales τ_{e}, τ_{R}, and τ_{d} are well separated. For smaller N, significant corrections must be expected. This has recently been demonstrated by a detailed theoretical analysis[31] of the Evans−Edwards model[29] and by comparison of the analytical results with the outcome of simulations.[30,32] The Evans−Edwards model is a lattice model, in which a single chain moves on a simple cubic lattice through impenetrable obstacles placed in the centers of each unit cell of the lattice (a monomer occupies one lattice site). These obstacles impose a strong geometric confinement on the motion of the chain: The tube diameter d_{T} is on the order of the lattice constant. Even under these very favorable conditions, long chains and long times are required to display the asymptotic power laws clearly.[30,32] If one wants to analyze the motion of the inner monomer in a different model, the experience with the studies of refs 30−33 suggests the use of the following three quantities: the mean-square displacement g_2, which behaves as

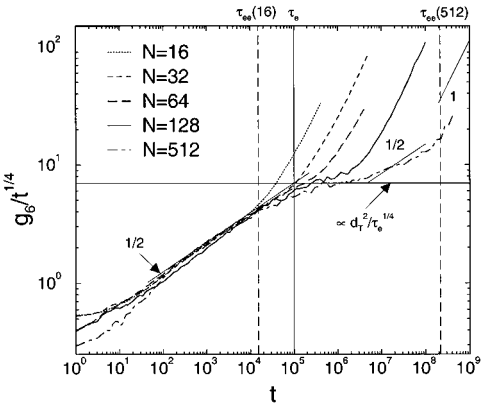

Figure 5. Time dependence of $g_6(t)/t^{1/4}$ for different chain lengths N. $g_6(t)$ is the cubic invariant defined by eq 9. This function is predicted to behave similarly to the mean-square displacement of an inner monomer $g_1(t)$, but to exhibit the characteristics of reptation more clearly than $g_1(t)$.[30−33] In the interval $200 \lesssim t \lesssim 5000$, $g_6(t)$ increases roughly as $t^{1/2}$. Then, it crosses over to a weaker time dependence which is compatible with $g_6(t) \sim t^{1/4}$ for $4 \times 10^5 \lesssim t \lesssim 2 \times 10^6$. The intersection between these two asymptotic power-laws provides an estimate for the entanglement time $\tau_{\mathrm{e}} \approx 100175$ (solid vertical line). Using eq 10, $g_6(\tau_{\mathrm{e}})/\tau_{\mathrm{e}}^{1/4} \simeq d_{\mathrm{T}}^2/3\tau_{\mathrm{e}}^{1/4} \approx 7$, the tube diameter is approximately given by $d_{\mathrm{T}} \approx 19.3$. Furthermore, the two dashed vertical lines indicate the values of the relaxation time, τ_{ee}, of the end-to-end vector, defined by eq 21, for $N = 16$ and $N = 512$.

$$
g_2(t) \sim \begin{cases} \sim g_2(t) & \text{if } t \ll \tau_{\mathrm{d}} \\ \rightarrow R_{\mathrm{g}}^{\,2} & \text{if } \tau_{\mathrm{d}} \ll t \end{cases} \tag{8}
$$

so that a transition from $g_2 \sim t^{1/4}$ and $g_2 \sim t^{1/2}$ cannot be interpreted as a crossover to free diffusion due to the saturation of g_2 at late times, the "cubic invariant"[30−33]

$$
g_6(t) = \sqrt{\left\langle \sum_{\alpha=1}^{3} [R_{\alpha,N/2}(t) - R_{\alpha,N/2}(0)]^4 \right\rangle} \sim g_1(t) \tag{9}
$$

which is predicted to be much less plagued than g_1 by preasymptotic corrections (for the Evans−Edwards model), and the ratio $g_4(t)/g_1(t)$. This ratio should start around 1 at early times, develop a maximum at intermediate times, and approach 1 if $t \rightarrow \infty$ (= free diffusive limit for both g_4 and g_1). For Rouse dynamics the maximum occurs at $t \lesssim \tau_{\mathrm{R}}$ and has the value $g_4/g_1 = 2$. If the chain reptates, the analysis of the Evans−Edwards model suggests that the position of the maximum is still given by $t \approx \tau_{\mathrm{R}}$, but its amplitude should be much larger than 2 ($g_4/g_1 \approx 4\sqrt{2}$ for $N \rightarrow \infty$).[31−33]

Figures 5 and 6 depict the time dependence of g_6 and g_2, respectively. The ordinates are divided by $t^{1/4}$ to highlight the expected asymptote for the onset of reptation. The figures show that the initial increase of g_6 and g_2, which is roughly compatible with a $t^{1/2}$-behavior for $200 \lesssim t \lesssim 5000$, considerably slows down when $t > 10^5$. However, an unambiguous indication of the $t^{1/4}$-power law is not visible. The simulation data

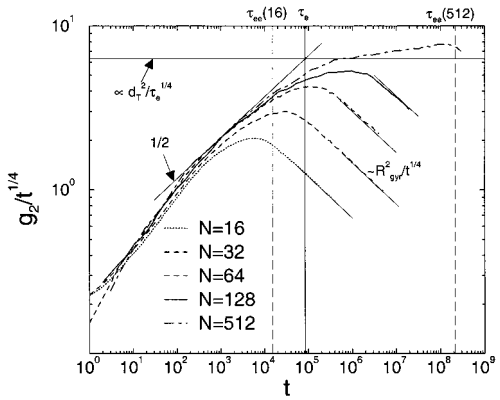

Figure 6. Time dependence of $g_2(t)/t^{1/4}$ for different chain lengths N. $g_2(t)$ is the displacement of an inner monomer relative to the chain's center of mass (eq 6). For times shorter than the Rouse, τ_R, or disentanglement time, τ_d, one expects $g_2(t) \sim g_1(t)$, whereas $g_2(t) \rightarrow R_g^2$ otherwise. Because of eq 22, these times can be represented by the relaxation time, τ_{ee}, of the end-to-end vector (defined by eq 21). The latter behavior is borne out for $t > \tau_{ee}$ (vertical dashed lines shown for $N = 16$ and 512 only). As in Figure 5 for g_6 ($\approx g_1$), there is an approximate $t^{1/2}$-increase for $200 \lesssim t \lesssim 5000$ which crosses over to a weaker time dependence. This weaker dependence is (perhaps) compatible with $g_2 \sim t^{1/4}$ for $N = 512$ over about half a decade ($5 \times 10^5 \lesssim t \lesssim 10^6$). Using this interval, the intersection with the extrapolation of the $t^{1/2}$-behavior yields estimates for the entanglement time, τ_e, and the tube diameter, d_T: $\tau_e \approx 84053$ (solid vertical line), $d_T \approx 18.6$ (via eq 10).

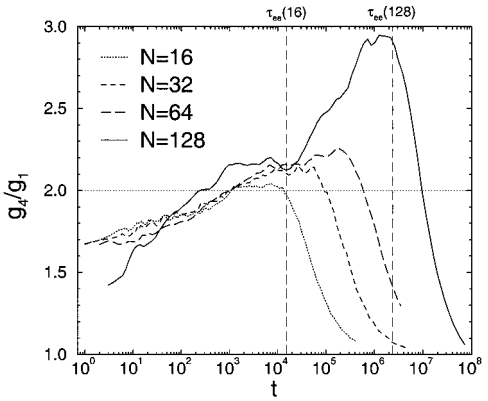

Figure 7. Ratio of the mean-square displacement of the end monomer, $g_4(t)$, and the inner monomer, $g_1(t)$, vs logarithm of time for different chain lengths N (see eq 6). The dashed vertical lines indicate the relaxation time, τ_{ee}, of the end-to-end vector for $N = 16$ and $N = 128$ (τ_{ee} is defined by eq 21; see Table 1). The vertical dotted line shows the value of the maximum, $g_4/g_1 = 2$, expected from the Rouse model. This maximum should occur for $t \lesssim \tau_R$. For a reptating chain, a maximum is still expected to occur at $t \approx \tau_R$, but to be much larger than 2.[31−33] The onset of this behavior is visible for $N = 128$. In the limit $t \rightarrow \infty$, both displacements become diffusive. So, $g_4/g_1 \rightarrow 1$. Since $g_4 \sim g_1$ in general, the calculation of the ratio g_4/g_1 eliminates the dominant variation with time and highlights the differences between both displacements. Thereby, statistical errors also become much better visible. For $N = 512$, they are so pronounced that a quantitative analysis was not possible.

rather exhibit a gradual crossover to a weaker time dependence which might approach $t^{1/4}$ if longer chains could be studied. This interpretation is suggested by the behavior of $N = 512$. Even for this chain length there is no clear sign of a subsequent $t^{1/2}$-increase, but only a fairly protracted transition to the large-time limits $g_6 \sim t$ and $g_2 \rightarrow R_g^2$. All other chain lengths already cross over to these limits for $t > 10^5$ (this is especially well visible for g_2). Therefore, much larger (or stiffer[36,55,56]) chains and still better statistics are needed to clearly separate the different power laws and to eventually distinguish between reptation theory and alternative approaches, such as polymer mode-coupling theory,[21−26] for instance.

To proceed with the analysis in the framework of reptation theory, we looked for that time regime which is best compatible with the predicted $t^{1/4}$-behavior. Then, estimates of the tube diameter d_T and the entanglement time τ_e can be obtained from the figures by posing

$$g_6(\tau_e) \simeq g_2(\tau_e) \simeq g_1(\tau_e) = \frac{{d_T}^2}{3} \qquad (10)$$

where τ_e is defined by the intersection point of the $t^{1/2}$- and $t^{1/4}$-power laws. The factor $^1/_3$ in eq 10 was proposed in refs 57 and 58 and justified by the following argument: The tube diameter can be interpreted as the end-to-end distance of a chain segment with N_e monomers. This is the largest segment which does not feel the entanglement constraint yet. It relaxes as a Rouse chain. So, $\tau_e = \tau_R(N_e)$ which gives $g_1(\tau_e) \approx {d_T}^2/3$.[4] Qualitatively, the factor $^1/_3$ also appears reasonable. If we assume that the end-to-end vector $\boldsymbol{d}_T^2$ is predominantly oriented along the tube axis, the average extension of the tube perpendicular to its axis should be proportional to the radius of gyration ${d_T}^2/6$ and thus smaller than ${d_T}^2$.[33]

If one accepts these arguments, eq 10 yields $d_T \approx 17.9$, 19.3 and $\tau_e \approx 84053$, 100175 for g_2 and g_6, respectively, so that on average $d_T \approx 18.6$ and $\tau_e \approx 92114$. Using the result for d_T, we can furthermore estimate the entanglement length N_e by requiring ${d_T}^2 = {R_e}^2(N_e)$. To this end, we fitted the simulation data for ${R_e}^2$ in the range $16 \leq N \leq 64$ by a power law, which gives ${R_e}^2(N) = 6.872N^{1.08}$ so that $N_e \approx 38$. This value is about 26% larger than the original estimate,[34] but coincides very well with the result of a recent study.[36]

Figure 7 shows the simulation results for the ratio of the mean-square displacement of the end monomer and the inner monomer, $g_4(t)/g_1(t)$. The ratio starts around 1.5 at early times, exhibits a maximum at intermediate times and tends to 1 for large t. For $N \leq 64$ the maximum occurs close to $g_4/g_1 = 2$, i.e., to the value expected from the Rouse model, whereas it is larger for $N = 128$ ($g_4/g_1 \approx 3$). An increase of the maximum beyond the Rouse limit with growing chain length is predicted theoretically for the Evans−Edwards model and proposed as a sensible indicator of reptation dynamics.[31−33] For a reptating chain the disparity between g_4 and g_1 has to increase because the motion of the inner monomer is strongly confined by the tube at intermediate times, whereas end monomers always take part in tube renewal. Our data for $N = 128$ are indicative of such an enhancement beyond the Rouse limit and are qualitatively similar to simulation results of the Evans−Edwards model with a randomly dilute obstacle lattice (see Figure 5 of[33]). Although random dilution does not remove the asymptotic reptational behavior of the Evans−Edwards model, ref 33 demonstrates that the chain length required to observe this behavior increases strongly with dilution. Unfortunately, we have to restrict our discussion to $N \leq 128$ because the calculation of the ratio g_4/g_1 makes the statistical inaccuracies become so pronounced that a quantitative analysis for

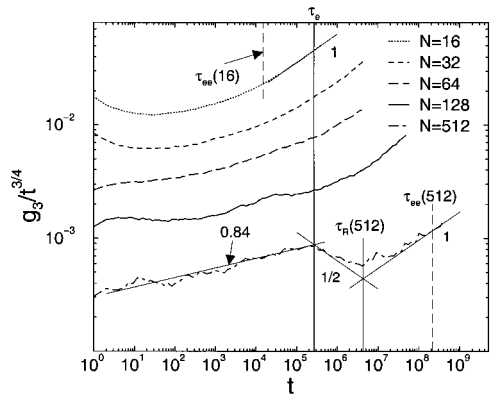

Figure 8. Time dependence of $g_3(t)/t^{3/4}$ for different chain lengths N. $g_3(t)$ is the mean-square displacement of the chain's center of mass (eq 6). Since reptation theory predicts a crossover from $g_3 \sim t^{1/2}$ for $\tau_e \lesssim t \lesssim \tau_R$ to $g_3 \sim t$ for $t > \tau_R$, $g_3(t)/t^{3/4}$ should exhibit a minimum at $t \simeq \tau_R$ and increase as $t^{-1/4}$ and $t^{1/4}$ for $t < \tau_R$ and $t > \tau_R$, respectively. Qualitatively, such a behavior is observed for $N = 512$ only (solid lines with slope $^1/_2$ and 1). The intersection point of both power laws yields an estimate for the Rouse time $\tau_R \approx 4.34 \times 10^6$, whence $d_T \approx 13$ by virtue of $g_3(\tau_R) = d_T^2/3$. The minimum is preceded by another power-law increase (empirically, $g_3 \sim t^{0.84}$) if $t \lesssim \tau_e$. For smaller chain lengths the power law is not as well pronounced. The intersection point of the power laws $g_3 \sim t^{0.84}$ and $g_3 \sim t^{1/2}$ yields another estimate of the entanglement time, $\tau_e \approx 268718$, and of the tube diamater, $d_T \approx 20.3$ (see eq 13). g_3 becomes diffusive in the range $t \approx \tau_{ee}$ (indicated by dashed vertical lines for $N = 16$ and 512; τ_{ee} relaxation time of the end-to-end vector, see eq 21).

$N = 512$ was not possible. However, even this chain length would certainly not be sufficient to provide clear evidence for reptation dynamics in our model, as Figures 5 and 6 already indicated.

In addition to the displacement of inner and end monomers the motion of the center of mass is also interesting. Figure 8 plots $g_3(t)/t^{3/4}$ vs time for all chain lengths studied. This representation of the ordinate was motivated by eq 7. If a chain reptates, $g_3(t)/t^{3/4}$ should exhibit a minimum close to $t = \tau_R$, which is preceded by a $t^{-1/4}$-descent and followed by a $t^{1/4}$-ascent. Similar to the findings for g_2 and g_6 there is no clear evidence for this scenario. A possible signature of it (perhaps) emerges for $N = 512$ only, whereas the transition to free diffusion intervenes for smaller chain lengths.

On the other hand, the data reveal that g_3 is subdiffusive at early times. In particular, for $N = 512$, where τ_e and the crossover-time to free diffusion are well separated, this behavior is very pronounced. The mean-square displacement increases as $g_3 \sim t^x$ with an effective exponent $x \approx 0.84$. Subdiffusive motion of the center of mass at early times is not unusual. It is generally found in computer simulations of linear polymers (see refs 11 and 12 for reviews and ref 59 for a chemically realistic model of polyethylene) and of rings,[60] and it has also been observed lately in experiments (on short chains).[54] The subdiffusive behavior should be considered as a condensed-phase effect. In a dense melt, a polymer is intermingled with many other chains. Their presence impedes the motion of the center of mass of the tagged chain, leading to subdiffusive behavior. Evidence for this interpretation is provided, for instance, by simulations at different densities. If the density decreases toward the single-chain limit, the bond-fluctuation model yields $g_3 \sim t$ for all times (i.e., typical Rouse behavior).[12,34,36] Another evidence stems from recent molecular dynamics simulations of the Kremer−Grest model.[61] In this study, the velocity−autocorrelation function of the center of mass was determined. The correlation function becomes negative at intermediate times and approaches 0 from below. This means that the surrounding polymers exert a force on the tagged chain, which reverses its velocity and tries to push it back to its original position.

Since the subdiffusive motion of g_3 is already present for short nonentangled chains, it should replace the expectation from the Rouse model $g_3 \sim t$ for $t < \tau_e$ (see eq 7). To analyze the time dependence of g_3, we proceeded in the same way as in the case of g_2 or g_6 by looking for that time window which is best compatible with the predicted $t^{1/2}$ behavior. Then, one can try to determine τ_e from the intersection of $g_3 \sim t^{0.84}$ and $g_3 \sim t^{1/2}$. This yields $\tau_e \approx 268\,718$, which is about a factor of 2.5 larger than the results derived from g_6 or g_2. Nevertheless, if one accepts this value, another estimate of d_T can be obtained by posing

$$g_3(\tau_e) = \frac{b^2\, d_T^{\,2}}{3R_e^{\,2}} \left(\frac{k_B T}{\zeta b^2}\, \tau_e\right)^{1/2} \tag{11}$$

where the factor $^1/_3$ stems from eq 10 and the requirement $g_1(\tau_d) = g_3(\tau_d)$. In eq 11, ζ denotes the monomeric friction coefficient and τ_e is (assumed to be) given by[12]

$$\tau_e = \left(\frac{d_T}{b}\right)^4 \frac{\zeta b^2}{k_B T} \tag{12}$$

so that

$$d_T = [3 g_3(\tau_e) R_e^{\,2}]^{1/4} \tag{13}$$

Using $g_3(\tau_e) \approx 10.37$ and $R_e^2 = 5348$, eq 13 leads to $d_T \approx 20.3$. This value is compatible with previous estimates from g_6 and g_2. However, due the small exponent $^1/_4$ in eq 13, the result for the tube diameter is not very sensible to variations of τ_e. For instance, when using the average τ_e from g_6 and g_2, i.e., $\tau_e \approx 92114$, so that $g_3(\tau_e) \approx 4.27$, one obtains $d_T \approx 16.2$, which is also in reasonable agreement with the results derived from the monomer displacements.

On the other hand, the power law $g_3 \sim t^{1/2}$ provides a further possibility to determine d_T by the intersection with the diffusive behavior $g_3 \sim t$. The intersection point should define the Rouse time τ_R ($\approx 4.34 \times 10^6$), and one expects the value $g_3(\tau_R)$ to be close to d_T^2. If we determine the prefactor by the same argument which led to eq 11, we obtain $g_3(\tau_R) \approx d_T^2/3$. Using $g_3(\tau_R) \approx 54.8$, we find $d_T \approx 13$. This value seems too small in comparison with the previous results, which indicate that the Rouse time is presumably larger than determined. Therefore, $\tau_R = 4.34 \times 10^6$ instead corresponds to a lower bound than to a reliable estimate.

B. Correlation Functions. If a chain starts to reptate, the motion of the monomers perpendicular to the primitive path is restricted to displacements smaller than the tube diameter. This implies that the decay of orientational correlation functions of chain segments should significantly slow if the size of the segment becomes comparable to d_T. Therefore, correlation functions which probe reorientations on different length scales along the backbone of a chain are interesting quantities.

The smallest segment along the backbone of a chain is the bond vector. The correlation function of the bond

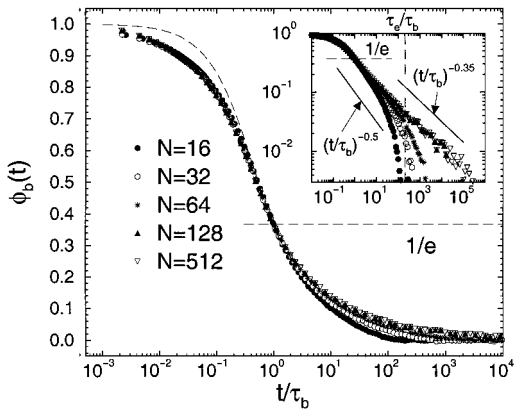

Figure 9. Scaling plot of the autocorrelation function, $\phi_b(t)$, of the bond vectors for different chain lengths vs t/τ_b. The relaxation time, τ_b, was defined by (see Table 1): $\phi_b(\tau_b) = 1/e$ (dashed horizontal lines in the main figure and the inset). This scaling collapses the correlators onto a master curve if $0.25 \lesssim \phi_b(t) \leq 1$. The final decay, $\phi_b(t) < 0.25$, depends on chain length. For $N = 16$, it is well described by the Rouse model, i.e., by eq 15 (dashed curve in the main figure), whereas eq 15 decays faster than the simulation data for $N \geq 32$. Especially, the largest chain lengths ($N = 128$, 512) exhibit a slow power-law decay (empirically, $\phi_b(t) \sim t^{-0.35}$), as illustrated in the inset. The inset also indicates the Rouse behavior, $\phi_b(t) \sim t^{-0.5}$, expected for $t < \tau_e$ ($\tau_e = 92\ 114$ = average entanglement time of Figures 5 and 6).

vector can be defined by

$$\phi_b(t) = \frac{1}{(N-1)l^2} = \sum_{n=1}^{N-1} \langle \boldsymbol{l}_n(t) \cdot \boldsymbol{l}_n(0) \rangle \qquad (14)$$

where $l^2 = \langle \boldsymbol{l}^2(0) \rangle$ is the mean-square bond length. This quantity is also interesting because it should be closely related to the shear modulus.[26] Figure 9 illustrates the time- and chain-length dependences of $\phi_b(t)$. The data are presented in a scaling plot where the time axis is given in units of the relaxation time, τ_b, of the bond vector defined by $\phi_b(\tau_b) = 1/e$. This time scale depends weakly on chain length (see Table 1). If τ_b was the only relevant time scale, all $\phi_b(t)$'s, measured for different N, should collapse onto a master curve. Figure 9 shows that such a collapse is realized for about 75% of the relaxation, whereas the final decay to zero depends on chain length. Larger chains relax more slowly than shorter ones.

Such a behavior is already expected from the (discrete[50]) Rouse model which expresses $\phi_b(t)$ as

$$\phi_b(t) = \frac{1}{N-1} \sum_{p=1}^{N-1} \phi_p(t) = \frac{1}{N-1} \sum_{p=1}^{N-1} \exp\left(-\frac{tp^2}{\tau_R}\right) \qquad (15)$$

where τ_R is the Rouse time and $\phi_p(t)$ the correlation function of the pth Rouse mode[4,50]

$$\phi_p(t) = \frac{\langle \boldsymbol{X}_p(t) \cdot \boldsymbol{X}_p(0) \rangle}{\langle \boldsymbol{X}_p{}^2(0) \rangle} = \exp\left(-\frac{tp^2}{\tau_R}\right) \qquad (16)$$

If $t \ll \tau_R$, the relaxation behavior of the sum in eq 15 is dominated by large p's, which yields $\phi_b(t) \sim 1/t^{1/2}$ independent of N (in the continuum limit). On the other hand, if $t \gtrsim \tau_R$, $\phi_b(t)$ relaxes more slowly, the longer the chain length. These predictions seem to be in accord with the simulation results. However, there are differences at short times for all chain lengths and at long times for large N.

At short times, the Rouse formula, eq 15, underestimates the relaxation strength of $\phi_b(t)$. This discrepancy is caused by eq 16 which assumes an exponential decay for all Rouse modes. However, especially the simulation results for large Rouse modes do not decay in a simple exponential fashion (see discussion of Figure 12). These large modes determine the behavior of $\phi_b(t)$ at short times, whereas the late-time relaxation is dominated by the smallest Rouse mode which is almost exponential for $N \leq 128$. Nevertheless, eqs 15 and 16 only provide a reasonable description for the N-dependent tail of $\phi_b(t)$ if $N = 16$. For larger N the simulation data relax more slowly and finally develop a power-law decay if $N \geq 128$. The power law starts around $t \approx \tau_e$ and extends over about 3 decades up to the end of our simulation. With the present simulation results we cannot decide whether the power law is an indication of a possible two-step relaxation, which would become clearly visible for longer chains, as suggested by polymer mode-coupling theory.[24,26]

Qualitatively, the slow power-law decay of $\phi_b(t)$ implies that some bonds lose the memory of their original orientation only very gradually. Persistence of bond orientation is also an important notion in the development of the continuum theory of reptation.[4] There, a key quantity is the probability $\psi(s,t)$ that a segment s of the primitive chain is still in the tube at time t. This probability is related to the projection of the (unit) tangent vectors, $\boldsymbol{u}(s',t)$, of all segments s' onto one primitive path segment s, i.e., onto $\boldsymbol{u}(s,0)$ (see eq 6.45 of ref 4). In analogy to $\psi(s,t)$, we define

$$\phi_n(t) = \frac{\sum_{n'=1}^{N} \langle \boldsymbol{l}_{n'}(t) \cdot \boldsymbol{l}_n(0) \rangle}{\sum_{n'=1}^{N} \langle \boldsymbol{l}_{n'}(0) \cdot \boldsymbol{l}_n(0) \rangle} \qquad (17)$$

which represents the probability that the original orientation of the bond vector $\boldsymbol{l}_n(0)$ is still present at time t. This quantity can be calculated by the (discrete[50]) Rouse model. The result is

$$\phi_n(t) = \frac{\sum_{p=1(\text{odd})}^{N-1} [\sin(np\pi/N)/\tan(p\pi/2N)] \exp(-p^2 t/\tau_R)}{\sum_{p=1(\text{odd})}^{N-1} \sin(np\pi/N)/\tan(p\pi/2N)} \qquad (18)$$

$$\overset{p/N \ll 1}{=} \frac{4}{\pi} \sum_{\substack{p=1 \\ (p\ \text{odd})}}^{\infty} \frac{1}{p} \sin(np\pi/N) \exp(-p^2 t/\tau_R) \qquad (19)$$

The continuum limit (19) is identical to the reptation formula for $\psi(s,t)$ if τ_R is replaced by the disentanglement time τ_d. Numerically, the discrete and continuum results for $\phi_n(t)$ are almost indistinguishable. Therefore, we compare eq 18 with simulation data for $N = 16$ and $N = 128$ in Figure 10.

If $N = 16$, eq 18 provides a fairly accurate description of the simulated $\phi_n(t)$. Both theory and simulation yield bell-shaped curves whose amplitudes become smaller

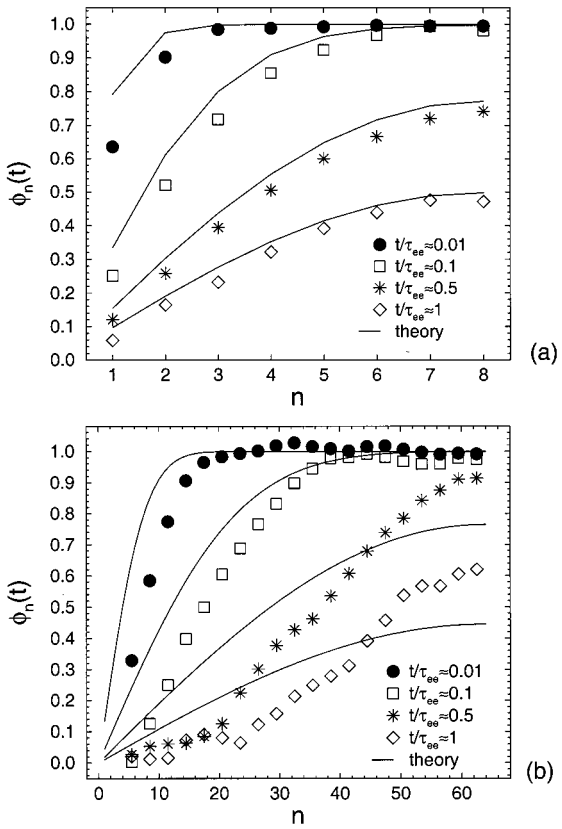

Figure 10. Survival probability 17, $\phi_n(t)$, of an initial bond vector $\boldsymbol{l}_n(0)$ for $N = 16$ (panel a) and $N = 128$ (panel b). $\phi_n(t)$ is plotted as a function of the bond number n. For example, $n = 1$ corresponds to the bond vector $\boldsymbol{l}_1(0)$ connecting the first and the second monomer. Time is measured in units of the relaxation time of the end-to-end vector τ_{ee} (see Table 1). The solid lines represent the prediction of eq 18. To improve the statistics, the simulation results were averaged over both halves of the chain—the chain is symmetric with respect to its ends. Therefore, results from $n = 1$ to $n = N/2$ are shown only. This was sufficient for the short chain, but not for $N = 128$. In this case, the bonds n and $n + 1$ were lumped additionally and the resulting average was plotted at the (nonexisting) bond number $n + {}^1/_2$.

as time increases. This behavior can be rationalized as follows: Since chain ends are more mobile than inner monomers, bond vectors close to the ends decorrelate more quickly than those in the inner part of the chain. The decorrelation thus propagates from the chain ends toward the middle monomer. The bond vector orientation of the inner monomer is rather long-lived. Even at $t = \tau_{ee}$, where the end-to-end vector correlation has decayed to about 30% of its original value (see eq 21 and Figure 11), $\phi_n(t)$ is still about 0.5 for $n = 8$. This slow relaxation is already present for short, Rouse-like chains and should not be considered as a characteristic feature of reptation-like dynamics, since the Rouse and reptation formulas agree with one another (eq 19).

However, the simulation results for $\phi_n(t)$ exhibit differences between short and long chains. As Figure 10 shows, the relaxation of inner monomers becomes strongly retarded compared to the theoretical (reptation) prediction if $N = 128$. More than 50% of the initial orientation of the inner third of the chain is preserved even at τ_{ee}. These long-lived correlations, which are not present for small N, should be responsible for the power-law behavior of $\phi_n(t)$ (see Figure 9) because they begin to develop in the same time window as the power law, i.e, for times larger than the entanglement time (τ_e/τ_{ee} ≈ 0.04 for $N = 128$), and last until $t > \tau_{ee}$ (the time $t/\tau_b = 10^4$ in Figure 9 corresponds to about $t/\tau_{ee} \approx 2$ in Figure 10b).

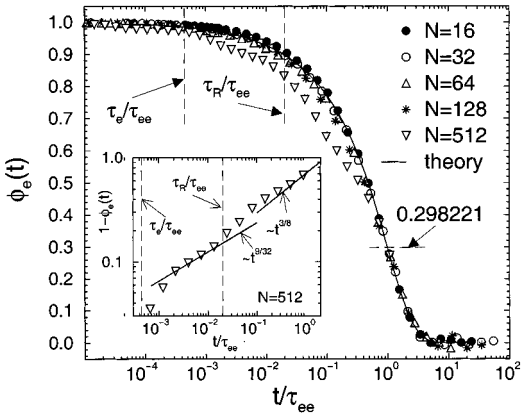

Figure 11. Autocorrelation function of the end-end vector, $\phi_e(t)$, vs scaled time t/τ_{ee} for all chain lengths studied. The scaling time, τ_{ee}, is defined by eq 21: $\phi_e(\tau_{ee}) = 0.298221$ (dashed horizontal line). The vertical dashed line indicates the value of the entanglement time τ_e (=92 114 = average τ_e from Figures 5 and 6) and of the Rouse time $\tau_R(N = 512)$ ($\approx 4.34 \times 10^6$) determined from Figure 8. Both times are divided by $\tau_{ee}(N = 512)$ (see Table 1). The solid line depicts the result of eq 20. The inset shows $1 - \phi_e(t)$ vs t/τ_{ee} for $N = 512$ together with the power laws $1 - \phi_e(t) \sim t^{9/32}$ and $1 - \phi_e(t) \sim t^{3/8}$ expected from polymer mode-coupling theory for $\tau_e \ll t \ll \tau_R$ and $\tau_R \ll t \ll \tau_{RR}$ (τ_{RR} renormalized Rouse time).[24]

Furthermore, they should also become visible in the motion of the monomers, particularly when comparing the mean-square displacement of the end monomer, $g_4(t)$, with that of the inner monomer $g_1(t)$. Figure 10 suggests that the ratio $g_4(t)/g_1(t)$ for $t \approx \tau_{ee}$ is much larger for $N = 128$ than for $N = 16$. Our simulation data for g_4/g_1 support this expectation (see Figure 7).

If the chain length increases, one may expect the slowly relaxing zone around the middle monomer to grow and to influence the dynamic behavior of the chain more and more. For instance, one might speculate that the end-to-end vector relaxes in two steps: There is a first step initiated by the chain ends. Their fast motion decorrelates adjacent bond vectors very efficiently. However, this decorrelation does not propagate homogeneously along the polymer backbone toward the inner monomer as it is the case for short chains, but slows down in the inner part of the chain. The relaxation of this part is responsible for the second step.

Some evidence for this conjecture is given in Figure 11, which shows the time dependence of the end-to-end vector correlation function, $\phi_e(t)$, for all chain lengths studied and compares the simulation data with the Rouse (or reptation) prediction

$$\phi_e(t) = \frac{\langle \boldsymbol{R}_e(t)\cdot\boldsymbol{R}_e(0)\rangle}{\langle \boldsymbol{R}_e(0)^2\rangle} = \sum_{\substack{p=1\\(p\ \mathrm{odd})}}^{\infty} \frac{8}{p^2\pi^2} \exp(-p^2 t/\tau_{ee}) \quad (20)$$

where the relaxation time τ_{ee} is defined by

$$\phi_e(\tau_{ee}) = \sum_{\substack{p=1\\(p\ \mathrm{odd})}}^{\infty} \frac{8}{p^2\pi^2} \exp(-p^2) = 0.298221 \quad (21)$$

Note that eq 20 is the same for both Rouse and reptation theory, the only difference being that τ_{ee} is the Rouse

time, τ_R, in the first case and the disentanglement time, τ_d, in the latter case, i.e.

$$\tau_{ee} = \begin{cases} \tau_R = \dfrac{1}{3\pi^2}\dfrac{\zeta b^2}{k_B T} N^2 & \text{if } N \ll N_e \\ \tau_d = \dfrac{1}{\pi^2}\dfrac{\zeta b^2}{k_B T}\dfrac{b^2}{{d_T}^2} N^3 & \text{if } N \gg N_e \end{cases} \tag{22}$$

where prefactors $1/3\pi^2$ and $1/\pi^2$ are taken from ref 4 (they have been set equal to 1 in the discussion of the mean-square displacements in section IIIA).

Equation 20 suggests that simulation data for $\phi_e(t)$ depend on N only via τ_{ee}. By using a rescaled time axis, t/τ_{ee}, it should be possible to superimpose all data onto a master curve which is given by eq 20. Figure 11 confirms this expectation if $N \leq 128$. For $N = 512$, however, the relaxation is more complicated. It seems to occur in two steps. The first step starts at about $t \approx \tau_e$, and the second takes place in the time window where g_3 crosses over to free diffusion, i.e., on the scale of the Rouse time τ_R (see Figure 8). This behavior is similar to that expected from polymer mode-coupling theory.[24−26] The theory predicts two power laws: $1 - \phi_e(t) \sim t^{9/32}$ for $\tau_e \ll t \ll \tau_R$ and $1 - \phi_e(t) \sim t^{3/8}$ for $\tau_R \ll t \ll \tau_{RR}$ (τ_{RR} = renormalized Rouse time $< \tau_d$). Our data are compatible with a $t^{9/32}$-behavior for about 1 decade ($0.002 \lesssim t/\tau_{ee} \lesssim 0.1$) and eventually with $t^{3/8}$ close to τ_{ee}. Of course, this can only be considered as an indication that these predictions might be relevant for our model. Clarification of this point requires a much better separation of the relevant time scales and thus simulations of longer chains. On the other hand, it is not obvious that eqs 20 and 21 are accurate for chain lengths in the crossover regime from Rouse to reptation behavior, although they describe both limiting cases of the simple Rouse and the "pure" (i.e., asymptotic) reptation theory. Certainly, a quantitatively reliable theoretical prediction for $\phi_e(t)$ as well as for τ_{ee} in the regime where N and N_e are comparable would be very desirable.

The observed two-steplike relaxation behavior is not limited to $\phi_e(t)$. It can also be observed for the correlation function of the Rouse modes $\phi_p(t)$. Figure 12 shows scaling plots of $\phi_p(t)$ for $N = 16$ and $N = 512$. As suggested by eq 16, the scaling time, τ_p, is defined by $\phi_p(\tau_p) = 1/e$. The figure illustrates that the first Rouse mode is almost exponential for $N = 16$, whereas the relaxation of higher modes becomes progressively non-exponential with increasing p (smaller distance along the chain backbone). However, the curves cannot be described (completely) by a stretched exponential. This would imply that the fast decay of, e.g., $p = 15$ for $\phi_e(t) > 1/e$ entails a correspondingly slower relaxation if $\phi_e(t) < 1/e$. Since the data splay out with increasing p at short times, they should also splay out at late times, but in reverse order. There is no indication of that behavior in Figure 12a. The interplay of chain stiffness and local excluded volume forces gives rise to a more complicated than stretched-exponential time dependence. The same behavior is also observed for a bead−spring model of short chains[62] and, to some extent, for $N = 512$ in Figure 12b. For large chains, however, there is another factor which may contribute: cross-correlations between Rouse modes. Figure 3 revealed that these can be as pronounced as the self-correlation if $p = N - 1$. Since $\phi_{p=1}(t)$ exhibits again the signature of a two-step relaxation, such as $\phi_e(t)$, this behavior could also influence the decay of $\phi_{p=511}(t)$.

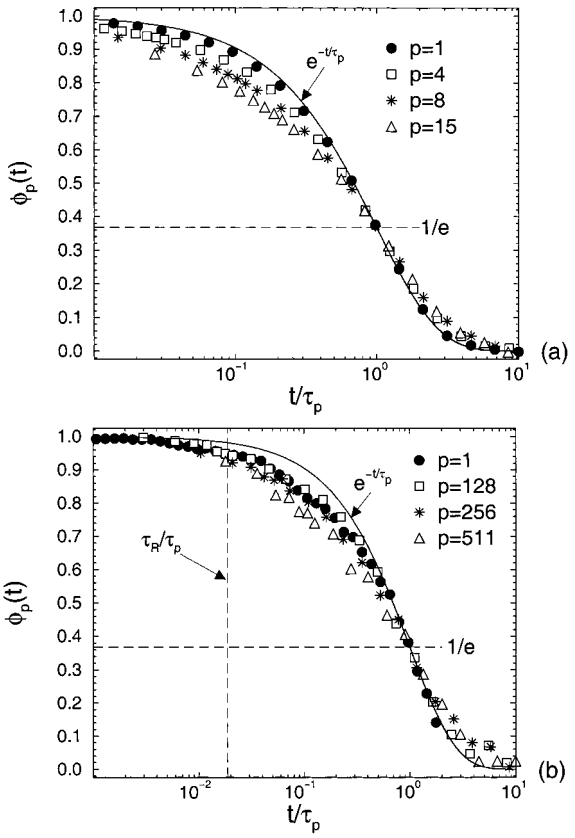

Figure 12. Correlation function of the Rouse modes, $\phi_p(t)$, vs rescaled time t/τ_p for $N = 16$ (panel a) and $N = 512$ (panel b). The scaling time, τ_p, is defined by: $\phi_p(\tau_p) = 1/e$ (dashed horizontal lines). For both chain lengths the relaxation of four representative mode indices p (=1, ..., $N - 1$) is shown. In addition, an exponential function (solid lines) is depicted. This is the behavior expected from the Rouse model (see eq 16). The vertical dashed line in panel b indicates the Rouse time $\tau_R(N = 512)$ ($\approx 4.34 \times 10^6$) determined from Figure 8. τ_R is divided by the relaxation time, τ_1, of the first Rouse mode (see Table 1).

C. Correlation Times and Diffusion Coefficient. The discrete Rouse model yields the following expression for the relaxation time τ_p[50]

$$\tau_p = \frac{1}{12}\frac{\zeta}{k_B T}\left[\frac{b}{\sin(p\pi/2N)}\right]^2 \tag{23}$$

$$= \frac{2}{3}\frac{N\zeta}{k_B T}\langle \boldsymbol{X}_p{}^2(0)\rangle \tag{24}$$

where eq 4 was used to obtain the last line. The unit of τ_p is set by the monomeric friction coefficient ζ which should be independent of the mode index p and chain length N. Within the framework of the Rouse model ζ can be determined from the diffusion coefficient, D, of a chain by

$$ND = \frac{k_B T}{\zeta} \tag{25}$$

If one furthermore identifies the effective bond length with $b^2 = R_e{}^2/(N - 1)$ (as already done in Figure 3), eq 23 suggests to construct a master curve by plotting $12DN(N - 1)\tau_p/R_e{}^2$ vs p/N. Figure 13 shows that such a

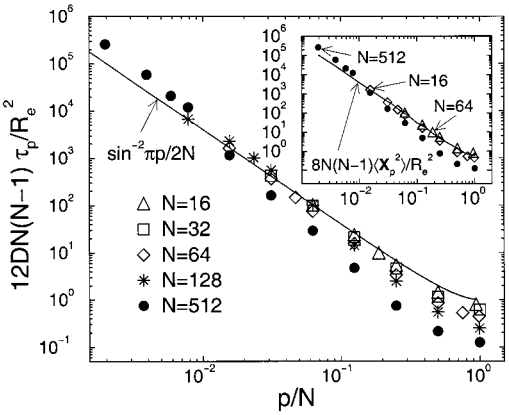

Figure 13. Variation of the Rouse mode relaxation time with the mode index p for different chain lengths N (entanglement length $N_e \approx 37$). The relaxation time, τ_p, is defined by the time value at which the correlation function of the Rouse modes has decayed to 1/e, i.e., $\phi_p(\tau_p) = 1/e$. Motivated by Rouse theory the abscissa and ordinate are scaled according to eq 23 where $\zeta b^2/k_BT$ is identified with $R_e^2/N(N-1)D$ (D = diffusion coefficient, see eq 25; R_e^2 = mean-square end-to-end vector). This scaling leads to a reasonable collapse if $N \leq 64$, whereas the p dependence for $N = 128$, 512 ($\gg N_e$) is s-shaped. τ_p is larger than the Rouse prediction (solid line) if p/N is small (especially for $N = 512$), but smaller than it for $p/N \to 1$. As for the static correlation $\langle \boldsymbol{X}^2(0)\rangle$ (see Figure 3), the Rouse model provides a good description of the p dependence if $p/N \lesssim 0.05$ (and $N \leq 64$), but overestimates the relaxation time for $p/N > 0.3$. The inset therefore tests whether τ_p can be written as $2\langle \boldsymbol{X}^2(0)\rangle/3D$ (see eq 24) with $\langle \boldsymbol{X}^2(0)\rangle$ taken from the simulation (see Figure 3). This is possible for $N \leq 64$, but not for large (entangled) chains, such as $N = 512$.

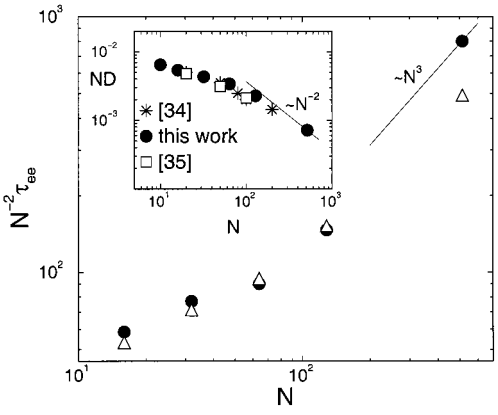

Figure 14. Chain length dependence of the end-to-end vector relaxation time, τ_{ee} (main figure), and of the diffusion coefficient, D, of a chain (inset). τ_{ee} and D are determined from eq 21 and from the long-time limit of g_3 ($=\lim_{t\to\infty} g_3(t)/6t$), respectively. Both quantities are scaled by the N dependences of eqs 22 and 25 to highlight deviations from Rouse behavior. The diffusion coefficient is compared with results from previous studies.[34,35] The solid lines in the main figure and the inset indicate the behavior, $\tau_{ee} \sim N^3$ and $D \sim N^{-2}$, suggested by reptation theory. The triangles (△) are the predictions of the Rouse formula $\tau_e = (Nb)^2\zeta/3\pi^2k_BT = R_e^2/3\pi^2D$, where the simulation results are used for D and R_e^2 (=end-to-end distance).

scaling is only possible if $N \leq 64$. For these chain lengths, the scaling yields a curve which is independent of N and coincides with the Rouse prediction for $p/N \lesssim 0.06$. On the other hand, there are deviations for $p/N \geq 0.3$, where eq 23 overestimates the simulation results.

Qualitatively, this behavior is identical to that observed for $\langle \boldsymbol{X}_p^2(0)\rangle$ in Figure 3. This suggests that the discrepancy between simulation and eq 23 might be related to local stiffness effects and that it could be removed by expressing $\langle \boldsymbol{X}_p^2(0)\rangle$ via eq 5 or by inserting the simulation results for $\langle \boldsymbol{X}_p^2(0)\rangle$ in eq 24. The latter choice was made in the inset of Figure 13. This yields a good description for $N \leq 64$. Two conclusions can be drawn from that: First, as expected from eq 24, $\langle \boldsymbol{X}_p^2(0)\rangle$ carries the whole p dependence so that ζ is constant. This should be considered as a property of the bond-fluctuation model and not as a general feature because a bead−spring model can exhibit a different behavior[62]. [This point was not stated explicitly in ref 62. However, since roughly $\langle \boldsymbol{X}_p^2(0)\rangle \sim p^{-2.2}$ and $\tau_p \sim p^{-2}$ in this case, eq 24 would imply $\zeta = \zeta_p \sim p^{0.2}$. Similar observations were also made in neutron scattering experiments on polyisobutylene.[53] A quantitative description of the experimental results was only possible if both local stiffness and an increase of ζ with increasing mode index p were taken into account.] Second, although the diffusion coefficients for $N \leq 64$ do not obey eq 25 [see Figure 14], the Rouse relation 24 effectively remains valid. This is possible because the simulation results for τ_p can be approximated by $\tau_p \propto f(N)[\sin(p\pi/2N)]^{-2}$ and the dependence of the function f on N is just given by $(N(N-1)D/R_e^2)^{-1}$. Theoretically, $N(N-1)D/R_e^2$ should represent the reorientation time of a monomer, $\zeta b^2/k_BT$, which is independent of N. In practice, $N(N-1)D/R_e^2$ varies from about 6×10^{-4} for $N = 16$ to about 3.5×10^{-4} for $N = 64$, i.e., by about 40%. For larger chain length, however, the residual N dependence of τ_p can no longer be lumped in a prefactor, although $N(N-1)D/R_e^2$ decreases to about 7×10^{-5} for $N = 512$ so that it is 1 order of magnitude smaller than for $N = 16$. Nonetheless, τ_p depends more strongly on N than $N(N-1)D/R_e^2$ for small p and $\tau_p/f(N)$ does not seem to be any longer a function of p/N alone. Even if one changes the prefactor to shift the data for $N = 128$ onto those for $N = 512$, one can guess from Figure 13 that such a collapse is only possible for $p/N \gtrsim 0.03$, whereas τ_p for $N = 512$ becomes larger than that for $N = 128$ when $p/N < 0.03$. Since scaling with p/N was possible for $\langle \boldsymbol{X}_p^2(0)\rangle$, which probes the static properties of a chain only, Figure 13 suggests that the friction coefficient ζ becomes p- and N-dependent.

Finally, Figure 14 shows the variation of τ_{ee} (defined by eq 21) and of D with chain length. The ordinates were scaled by the chain length dependence expected from the Rouse model, i.e., τ_{ee}/N^2 and ND (see eqs 22 and 25). The figure illustrates that neither τ_{ee} nor D behaves in a Rouse-like manner for small N or a reptation-like manner for large N. A possible explanation for this finding is given by a recent reanalysis[36] of the crossover scaling from the semidilute-solution to the melt state of the bond-fluctuation model.[34] This new analysis focused on the diffusion coefficient but substantially varied chain stiffness, which had not been done before. The important outcome for the present work is that the diffusion data of Figure 14 just lie in the crossover regime between Rouse dynamics, which is realized by flexible chains in dilute solution, and reptation dynamics, which is most pronounced for stiff chains in the melt. Apparently, chain stiffness reduces the tube diameter and thereby amplifies the reptation behavior. The same conclusion has also been suggested by a recent molecular-dynamics simulation of the Kremer−Grest model.[55] Since the diffusion data belong to the crossover regime, this should also hold for τ_{ee} in Figure 14 so that neither $\tau_e \sim N^2$ nor $\tau_{ee} \sim N^3$ can be observed. If one just fitted the last two chain lengths ($N = 128$, 512) by a power

law, one would obtain $\tau_{ee} \sim N^{3.23}$. This is similar to experiments where one often finds that the relaxation time scales as $N^{3.4}$.[5,6] Of course, the present simulation data cannot prove, but only provide an indication, that the bond-fluctuation model approaches (the possible asymptotic behavior) $\tau_{ee} \sim N^3$ from below with an exponent larger than 3, as suggested theoretically.[4,16,31] These theoretical studies show that the crossover to the reptation asymptote is postponed to very large N. To observe this asymptote one has to study either much longer or (eventually) stiffer chains which seem to show a clearer signature of reptation for accessible chain lengths.[36,55]

Nevertheless, one can use the simulation results for τ_{ee} to estimate the entanglement length N_e by requiring that τ_e corresponds to the relaxation time of a chain with end-to-end vector $d_T^2 = R_e^2(N_e)$. To read off N_e, we fitted τ_{ee} in the range of τ_e (=92 114), i.e., for $16 \le N \le 64$, by a power law. This gives $\tau_{ee} = 24.71N^{2.31}$ so that $N_e \approx 35$. This value is compatible with our previous estimate from $d_T^2 = R_e^2(N_e)$, i.e., $N_e \approx 38$ (see section IIIA), so that on average $N_e \approx 37$. This result agree very well with that obtained by the above-mentioned reanalysis of the crossover scaling.[36]

IV. Conclusions

The present paper summarizes an attempt to extend previous work[12,34,35] on the dynamics of long chain polymer melts toward larger chain lengths and longer times. The aim was to sufficiently enter the regime where entanglements should dominate the dynamics. However, it turned out that the crossover from nonentangled to entangled dynamics is very gradual. Even the longest chain, $N = 512$, which is about 14 times larger than the entanglement length, N_e, can only be considered as slightly entangled when analyzed in terms of the asymptotic power laws of reptation theory. This finding is expected from a theoretical analysis of the Evans−Edwards model[30−33] and molecular dynamics simulations.[57,58]

Reptation theory predicts that that there is an entanglement time τ_e, above which the mean-square displacements of inner monomers, $g_1(t)$ [$\approx g_6(t)$] and $g_2(t)$, and that of the center of mass, $g_3(t)$, increase as $\sim t^{1/4}$ and $\sim t^{1/2}$, respectively. Our data provide no clear evidence for this behavior but only a weak indication for $N = 512$ that it might (perhaps) become correct if longer chains could be studied. The analysis in the framework of reptation theory was thus performed with the results for $N = 512$ which are closest to the predicted behavior.

From the mean-square displacements, the tube diameter d_T and τ_e can be estimated: $d_T \approx 18.6$ and $\tau_e \approx 92\ 114$. Using these values and requiring $R_e^2(N_e) = d_T^2$ and $\tau_{ee}(N_e) = \tau_e$, the entanglement length may be read off of the simulation data: $N_e \approx 37$. The quoted values for d_T and τ_e are averages derived from g_2 and g_6. The results from g_2 and g_6 were rather close, whereas those from g_3 sometimes deviate substantially and thus appear to be less reliable (perhaps due to preasymptotic effects, as pointed out in ref 33). Of course, there are uncertainties connected with these numbers, especially with d_T, since the prefactors are unknown and $N = 512$ is not asymptotic. Here, the important point is that they are consistent with one another and with other independent studies. For instance, the value $N_e \approx 37$ agrees very well with that found in ref 36.

In addition to mean-square displacements, the orientational correlation functions of the bond vector, the end-to-end vector, and the Rouse modes were also studied. Bond vectors in the innermost part of a chain decorrelate from their initial orientations more slowly than bonds close to the ends. This difference is present for all chain lengths, but becomes much more pronounced if $N \gg N_e$ and $\tau_e \ll t \ll \tau_{ee}$. If there was a confining tube around a chain, such a behavior would be expected because reorientations of inner monomers are strongly hindered as long as the geometric constraints exist (i.e., for $t < \tau_{ee}$), whereas chain ends always take part in tube renewal and thus dissolve the confinement immediately. The simulations suggest that sensible indicators of this behavior could be a late-time power law decay of the bond-vector correlation function and a modulated (eventually two-step) relaxation of the end-to-end vector or Rouse modes correlation functions as well as the ratio $g_4(t)/g_1(t)$, as proposed in refs 31−33. The challenging problem consists of determining these functions with sufficient statistical accuracy in the relevant range of chain lengths and times.

For short chains ($N \lesssim N_e$) the Rouse model represents a viable, though not perfect, approach. Deviations are observed particularly on short length scales along the polymer backbone. This is to be expected because the microscopic potentials of the polymer should strongly influence the local dynamics. In general, these potentials cannot be represented by a flexible concatenation of Rousian harmonic springs but do introduce some local stiffness. If stiffness is taken into account, one can obtain a (almost) quantitative description of the static correlation $\langle \boldsymbol{X}_p^2(0) \rangle$ (for all N studied) and of the p dependence of the Rouse modes' correlation time τ_p, which scales as $\tau_p \sim \langle \boldsymbol{X}_p^2(0) \rangle$ (for $N \le 64$). Whereas the former property could be a general feature, the scaling $\tau_p \sim \langle \boldsymbol{X}_p^2(0) \rangle$ is certainly a property of our model. Simulations of other models[62] and neutron scattering experiments on polyisobutylene[53] suggest that the monomeric friction coefficient can be mode dependent. Such findings are plausible because one would in general not expect that static properties can uniquely determine the dynamic behavior. On the other hand, if $N \gg N_e$, our simulation results can also be interpreted as an indication for a p- and N-dependent friction coefficient.

Another characteristic dynamic property of the Rouse modes is the progressive nonexponential character of the relaxation with increasing mode index p. This behavior is not a special feature of the bond-fluctuation model, but is also observed for a bead−spring model[62] and in chemical realistic simulations of polyethylene.[59] These deviations from a pure exponential decay are important if one wants to calculate the relaxation of quantities, for which large modes and short times also contribute significantly. An example is provided by the bond-vector correlation function (see Figure 9). If one inserts the simulated Rouse modes instead of eq 16 into eq 15, a perfect description of the correlation function is obtained. Since this description only requires the orthogonality of the Rouse modes, it shows that the melt dynamics does not introduce (significant) correlations between different Rouse modes, i.e., $\langle \boldsymbol{X}_p(t) \cdot \boldsymbol{X}_q(0) \rangle \propto \delta_{pq}$. We believe that this property is general, since it is also observed for other models.[62]

A further important feature is that there is no significant regime of chain lengths where the Rouse prediction $D \sim 1/N$ holds (see inset of Figure 14).

Furthermore, the related prediction $g_3(t) \sim t$ (for $t \gtrsim 1$ in our units) is also not valid, not even for $N = 16$ (see Figure 8). If $g_3(t) \sim t$ were true, the log−log plot $g_3/t^{3/4}$ vs t should exhibit a straight line with slope $^1/_4$. However, we find a curved behavior spread over several decades. Our results (Figure 14) imply that there are about two decades in chain length ($10 \leq N \leq 10^3$) which are fully described neither by the simple Rouse model nor by asymptotic reptation theory or any other theory dealing with asymptotic power laws only. A more complete theoretical description including various crossovers suitable for explicit comparison with our (or other) model calculations is thus called for. This might also indicate which crossover behavior is universal and what the influences of the miscroscopic architecture (e.g., packing effects, stiffness, etc.) are.

Acknowledgment. We are indebted to J.-L. Barrat, R. Everaers, F. Eurich, M. Fuchs, P. Maass, C. Mischler, W. Paul, L. Schäfer, K. S. Schweizer, and J. Wittmer for helpful discussions on various aspects of this work. This study would not have been possible without a generous grant of simulation time by the HLRZ Jülich, the RHRK Kaiserslautern, the IDRIS Orsay, and the computer center at the University of Mainz. Financial support by the ESF Program on "Experimental and Theoretical Investigation of Complex Polymer Structures" (SUPERNET) is gratefully acknowledged.

References and Notes

(1) de Gennes, P. G. *J. Chem. Phys.* **1971**, *55*, 572.
(2) de Gennes, P. G. *J. Phys.* **1981**, *42*, 735.
(3) de Gennes, P. G. *Scaling Concepts in Polymer Physics*; Cornell University Press: Ithaca, NY, 1979.
(4) Doi, M.; Edwards, S. F. *The Theory of Polymer Dynamics*; Oxford University Press: New York, 1986.
(5) Graessley, W. W. *Adv. Polym. Sci.* **1982**, *47*, 68.
(6) Lodge, T. P.; Rotstein, N. A.; Prager, S. *Adv. Chem. Phys.* **1990**, *79*, 1.
(7) Ewen, E.; Richter, D. *Adv. Polym. Sci.* **1997**, *134*, 1.
(8) Pahl, S.; Fleischer, G.; Fujara, F.; Geil, B. *Macromolecules* **1997**, *30*, 1414.
(9) Welp, K. A.; Wool, R. P.; Satija, S. K.; Pispas, S.; Mays, J. *Macromolecules* **1998**, *31*, 4915.
(10) Baumgärtner, A. *Annu. Rev. Phys.* **1984**, *35*, 419.
(11) Kremer, K.; Grest, G. S. In *Monte Carlo and Molecular Dynamics Simulations in Polymer Science*; Binder, K., Ed.; Oxford University Press: New York, 1995; pp 194−271.
(12) Binder, K.; Paul, W. *J. Polym. Sci. B* **1997**, *35*, 1.
(13) Semenov, A. N.; Rubinstein, M. *Eur. Phys. J. B* **1998**, *1*, 87.
(14) Doi, M. *J. Polym. Sci.* **1983**, *21*, 667.
(15) Milner, S. T.; McLeish, T. C. B. *Phys. Rev. Lett.* **1998**, *81*, 725.
(16) McLeish, T. C. B.; Milner, S. T. *Adv. Polym. Sci.* **1999**, *143*, 195.
(17) de Gennes, P. G. *Macromolecules* **1976**, *9*, 587; 594.
(18) Daoud, M.; de Gennes, P. G. *J. Polym. Sci. Phys. Ed.* **1979**, *17*, 1971.
(19) Rubinstein, M.; Obukhov, S. P. *Phys. Rev. Lett.* **1993**, *71*, 1856.
(20) Semenov, A. N. *Physica A* **1990**, *166*, 263.
(21) Schweizer, K. S. *J. Chem. Phys.* **1989**, *91*, 5802; 5822.
(22) Schweizer, K. S. *Phys. Scr.* **1993**, *49*, 99.
(23) Schweizer, K. S.; G. Szamel, G. *Trans. Theor. Stat. Phys.* **1995**, *24*, 947.
(24) Schweizer, K. S.; Fuchs, M.; Szamel, G.; Guenza, M.; Tang, H. *Macromol. Theory Simul.* **1997**, *6*, 1037.
(25) Fuchs, M.; Schweizer, K. S. *Macromolecules* **1997**, *30*, 5133; 5156.
(26) Fuchs, M.; Schweizer, K. S. *J. Chem. Phys.* **1997**, *106*, 347.
(27) Shaffer, J. S. *J. Chem. Phys.* **1994**, *101*, 4205; **1995**, *103*, 761.
(28) Herman, M. F. *J. Chem. Phys.* **1990**, *92*, 2043; *Macromolecules* **1992**, *25*, 4925; 4391. Szleifer, I.; Loring, R. F. *J. Chem. Phys.* **1995**, *95*, 2080. Wilson, J. D.; Loring, R. F. *J. Chem. Phys.* **1992**, *97*, 3710; **1993**, *99*, 7150.
(29) Evans, K. E.; Edwards, S. F. *J. Chem. Soc., Faraday Trans.* **1981**, *2*, 1891.
(30) Ebert, U.; Baumgärtner, A.; Schäfer, L. *Phys. Rev. Lett.* **1997**, *78*, 1592.
(31) Ebert, U.; Schäfer, L.; Baumgärtner, A. *J. Stat. Phys.* **1998**, *90*, 1325.
(32) Baumgärtner, A.; Ebert, U.; Schäfer, L. *J. Stat. Phys.* **1998**, *90*, 1375.
(33) Schäfer, L.; Baumgärtner, A.; Ebert, U. *Eur. Phys. J. B* **1999**, *10*, 105.
(34) Paul, W.; Binder, K.; Heermann, D. W.; Kremer, K. *J. Phys. II* **1991**, *1*, 37. Paul, W.; Binder, K.; Heermann, D. W.; Kremer, K. *J. Chem. Phys.* **1991**, *95*, 7726.
(35) Wittmer, J.; Paul, W.; Binder, K. *Macromolecules* **1992**, *25*, 7211. Wittmer, J.; Paul, W.; Binder, K. *J. Phys. II Fr.* **1994**, *4*, 873.
(36) Müller, M.; Wittmer, J.; Barrat, J.-L. *Europhys. Lett.* **2000**, *52*, 406.
(37) Kremer, K.; Binder, K. *Comput. Phys. Rep.* **1988**, *7*, 259.
(38) Binder, K. In *Monte Carlo and Molecular Dynamics Simulations in Polymer Science*; Binder, K., Ed.; Oxford University Press: New York, 1995; pp 3−46.
(39) Deutsch, H. P.; Binder, K. *J. Chem. Phys.* **1991**, *94*, 2294.
(40) Baschnagel, J.; Paul, W.; Tries, V.; Binder, K. *Macromolecules* **1998**, *31*, 3856.
(41) Flory, P. J. *Statistical Mechanics of Chain Molecules*; Wiley: New York, 1969.
(42) Cannon, J. W.; Aronovitz, J. A.; Goldbart, P. *J. Phys. I* **1991**, *1*, 629.
(43) Aronovitz, J. A.; Nelson, D. R. *J. Phys.* **1986**, *47*, 1445.
(44) Rudnick, J.; Gaspari, G. *J. Phys. A: Math. Gen.* **1986**, *19*, 191.
(45) Šolc, K.; Stockmayer, W. H. *J. Chem. Phys.* **1971**, *54*, 2756. Šolc, K. *J. Chem. Phys.* **1971**, *55*, 335.
(46) Janszen, H. W. H. M.; Tervoort, T. A.; Cifra, P. *Macromolecules* **1996**, *29*, 5678.
(47) Eurich, F.; Maass, P. Soft Ellipsoid Model for Gaussian Polymer Chains [cond-mat/0008425].
(48) Murat, M.; Kremer, K. *J. Chem. Phys.* **1998**, *108*, 4340.
(49) Baschnagel, J.; Binder, K.; Doruker, P.; Gusev, A. A.; Hahn, O.; Kremer, K.; Mattice, W. L.; Müller-Plathe, F.; Murat, M.; Paul, W.; Santos, S.; Suter, U. W.; Tries, V. *Adv. Polym. Sci.* **2000**, *152*, 41.
(50) Verdier, P. H. *J. Chem. Phys.* **1966**, *45*, 2118.
(51) Allegra, G.; Ganazzoli, F. *Adv. Chem. Phys.* **1989**, *75*, 265.
(52) Harnau, L.; Winkler, R. G.; Reineker, P. *Europhys. Lett.* **1999**, *45*, 488.
(53) Richter, D.; Monkenbusch, M.; Allgeier, J.; Arbe, A.; Colmenero, J.; Farago, B.; Cheol Bae, Y.; Faust, R. *J. Chem. Phys.* **1999**, *111*, 6107.
(54) Smith, G. D.; Paul, W.; Monkenbusch, M.; Richter, D. *Chem. Phys.* **2000**, *261*, 61.
(55) Faller, R. Chain stiffness intensifies the reptation characteristics of polymer dynamics in the melt [cond-mat/0005192].
(56) Faller, R.; Müller-Plathe, F.; Heuer, A. *Macromolecules* **2000**, *113*, 6264.
(57) Kremer, K.; Grest, G. S. *J. Chem. Phys.* **1990**, *92*, 5057.
(58) Pütz, M.; Kremer, K.; Grest, G. S. *Europhys. Lett.* **2000**, *49*, 735.
(59) Paul, W.; Smith, G. D.; Yoon, Do Y. *Macromolecules* **1997**, *30*, 7772.
(60) Müller, M.; Wittmer, J. P.; Cates, M. E. *Phys. Rev. E* **1996**, *53*, 5063.
(61) Pütz, M. Dissertation (Mainz, 1999; unpublished).
(62) Bennemann, C.; Baschnagel, J.; Paul, W.; Binder, K. *Comput. Theo. Polym. Sci.* **1999**, *9*, 217.

MA001500F